
Interpretability-Guided Layer Selection over Subspace Projection: SAEs as Stethoscopes, Not Scalpels, for Raw Task Vector Model Editing

Li Lei
Incept Labs
Houston, TX

Madalina Ciobanu
Incept Labs
Houston, TX

Qingqing Mao*
Incept Labs, Houston, TX
Titan Holdings, San Francisco, CA
qmao@inceptlabs.ai

Ritankar Das
Incept Labs, Houston, TX
Titan Holdings, San Francisco, CA

Abstract

Large language models (LLMs) increasingly require surgical model editing to enhance domain-specific capabilities without incurring the computational cost or catastrophic forgetting associated with full fine-tuning. Sparse Autoencoders (SAEs) have emerged as a promising tool in this setting, in principle allowing for feature-level identification of where to intervene. In this work, we rigorously evaluate an SAE-guided editing pipeline for mathematical reasoning on Gemma-3-4B-IT and uncover a fundamental failure mode: **the intuitively appealing approach of projecting task vectors onto SAE feature subspaces acts as an information bottleneck that discards approximately 97% of the modification energy**, yielding no statistically significant improvements across seven math subjects. We show that this failure stems from a *geometric misalignment* between activation-space SAE directions and weight-space task vectors. We then propose a shift in perspective: **SAE as a Stethoscope, Not a Scalpel**, where SAEs are used for *layer-level diagnosis* rather than *intervention-level filtering*. By injecting unfiltered raw task vectors only into layers identified by an SAE-derived specificity score, we improve Number Theory accuracy from 29.6% to 39.4% ($z = +3.41$, $p = 0.0007$) on the Minerva Math benchmark, with 5 of 7 subjects significantly improved and none significantly degraded. Our method is fully deterministic, requires no additional inference cost, and provides a principled framework for interpretability-guided model editing.

1 Introduction

Large language models (LLMs) increasingly require *surgical model editing*: modifying only the components responsible for a target capability while leaving everything else intact. Standard adaptation methods such as LoRA [1] modify weights indiscriminately across all layers, leading to interference and catastrophic forgetting. Two largely separate research threads have pursued the surgical alternative. *Task arithmetic* [2] treats the weight difference between a fine-tuned model and its base as an additive “task vector” that can be composed, negated, or selectively reapplied in weight space. *Mechanistic interpretability* (MI) instead works in activation space, decomposing hidden representations into interpretable features—most prominently via Sparse Autoencoders (SAEs) [3, 4]—and intervening on those features to steer model behavior.

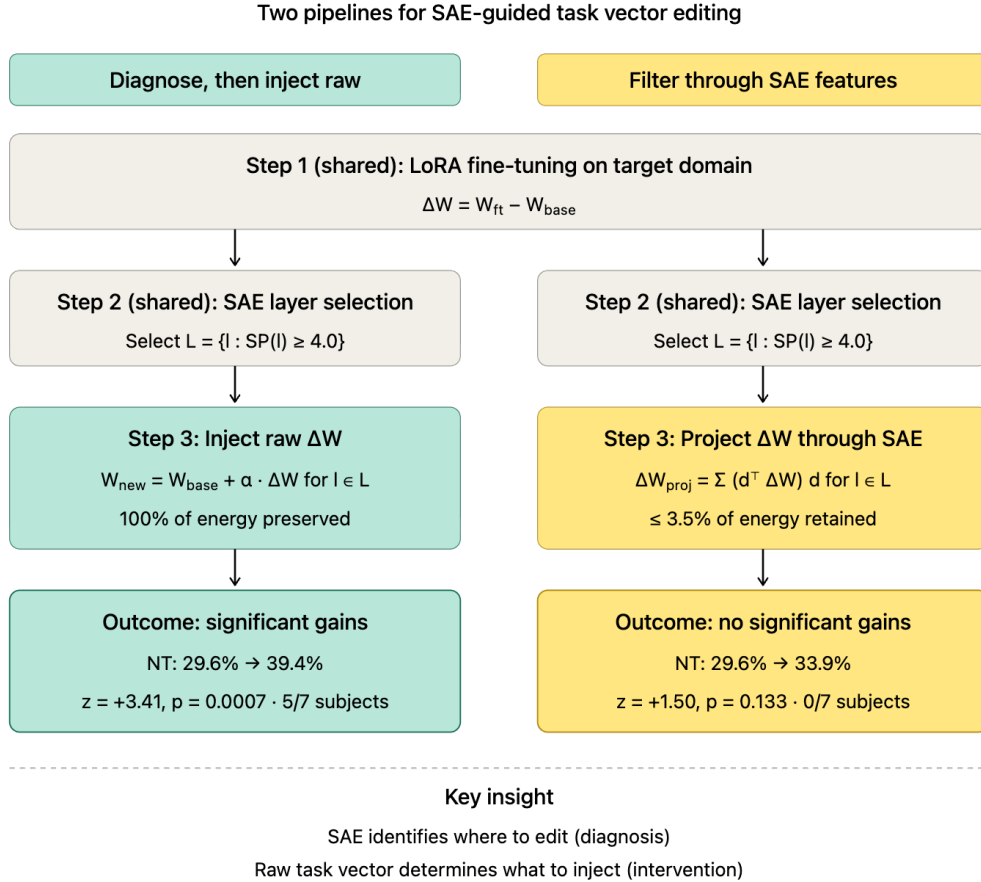


Figure 1: Two pipelines for SAE-guided task vector model editing. Both share Steps 1 (LoRA fine-tuning) and 2 (SAE layer selection); they differ only in Step 3. *Diagnose, then inject raw* (left) injects the unfiltered task vector ΔW into SAE-selected layers, preserving 100% of the modification energy. *Filter through SAE features* (right) projects ΔW onto the subspace spanned by domain-specific SAE decoder vectors, retaining only a few percent ($\leq 3.5\%$) of the energy. The former produces statistically significant gains on 5 of 7 math subjects; the latter produces none.

The intersection of these threads suggests a compelling pipeline: use SAEs to identify domain-relevant features, then inject task vectors *only through those features*. Pre-trained SAEs at scale, such as Gemma Scope [5] and Gemma Scope 2 [6], make this practical to implement off the shelf. Figure 1 contrasts this projection-based recipe with the alternative we propose.

A counterintuitive finding. We implement and rigorously evaluate this projection-based pipeline on Gemma-3-4B-IT [7] for mathematical reasoning and report a surprising negative result. **Projecting task vectors onto SAE decoder subspaces retains only a few percent ($\leq 3.5\%$) of the energy (discarding the remainder to 100%) and yields no statistically significant gains on any of seven math subjects.** Increasing the SAE feature width from 16K to 262K does not close the gap, indicating the bottleneck is intrinsic to projection rather than feature granularity. The failure has a clean mechanistic explanation: SAE decoder vectors $d_{l,j}$ live in *activation space* and capture statistical regularities of how the model represents information; task vectors ΔW live in *weight space* and encode how computations change. Projecting weight-space modifications through activation-space directions conflates two fundamentally different geometric structures, leading to near-total loss of functional signal [8].

This pattern is consistent with recent work questioning whether SAE-based interventions are reliable beyond probing. Sharkey et al. [8] catalogue substantial limitations of sparse dictionary learning.

Kantamneni et al. [9] show that SAE-based probes do not consistently outperform simple linear baselines. Heap et al. [10] find that SAEs trained on randomly initialized transformers produce features indistinguishable from those trained on real models. Concurrent work on protein language models reports that activation-space SAE editing and weight-space task arithmetic are *complementary* rather than substitutable, controlling different properties [11]. Together these results suggest the activation/weight distinction is a load-bearing axis of the editing problem.

SAE as stethoscope, not scalpel. Our central methodological claim is that SAEs are valuable as a *diagnostic* tool, not an *intervention* tool. We compute a per-layer specificity score (SP) derived from SAE feature analysis to identify domain-specialized layers, then selectively inject the unfiltered task vector into this subset. Notably, we identify an **empirical conservation of the modification budget**: as the number of selected layers decreases, the optimal scaling parameter α increases proportionally to maintain functional impact ($n_{layers} \times \alpha_{opt} \approx 11.2$). This separation preserves 100% of the modification energy in target layers while confining edits to the model’s domain-relevant regions.

Contributions. (i) We propose *SAE-Guided Layer Selection with Raw Task Vector Injection* and show on Minerva Math [12] that it improves Number Theory accuracy from 29.6% to 39.4% ($z = +3.41, p = 0.0007$), with 5 of 7 math subjects significantly improved and none significantly degraded. (ii) We document a substantive negative result: SAE projection of task vectors discards $\sim 97\%$ of the modification energy and produces no significant gains, even with a $16\times$ larger SAE—consistent with recent concerns about SAEs as intervention tools [8–10]. This negative result is the central scientific contribution of this work; the positive method (Section 3) is a constructive corollary that demonstrates SAE diagnostic utility separately from the failed projection approach. (iii) We provide 30+ ablation configurations, including alpha response curves, layer-selection strategies, multiple task vector sources, and dual-domain injection; extended ablations and reproduction details are in the appendix. We discuss limitations in Section 7.

2 Related Work

Task arithmetic and weight-space model editing. Ilharco et al. [2] introduced task vectors as the weight difference between models. Subsequent work addresses interference when combining multiple vectors, including TIES-Merging [13], DARE [14], Localize-and-Stitch [15], and Subspace Boosting [16]. While ROME [17] and MEMIT [18] utilize *causal tracing* to locate factual associations, our method provides a **fully deterministic, training-free diagnostic** for identifying domain-level specialization. This aligns with the findings of Ortiz-Jiménez et al. [19], who established that **weight disentanglement** is the crucial factor for effective task arithmetic. Our SAE-guided selection provides a principled criterion for isolating these task-relevant updates.

Sparse autoencoders and their limitations. SAEs decompose neural network activations into sparse, monosemantic features [3, 4], with comprehensive open suites available for the Gemma family [5, 6] and Llama family [20]. Recent work documents fundamental limitations: SAE reconstruction systematically loses information [8]; concepts may be convex regions rather than linear directions [21]; SAEs assume i.i.d. activations, ignoring sequential dependencies relevant to chain-of-thought reasoning [22]; SAE-based probes do not consistently outperform simple baselines [9]; and SAEs trained on randomly initialized transformers learn features qualitatively similar to those from trained models [10].

Weight-space vs. activation-space interventions. JoLA [23] jointly learns intervention locations and parameters in activation space. Katki et al. [11] find that for protein language models, weight-space task arithmetic and activation-space SAE editing are complementary, each more effective for a different subset of biochemical properties. Our paper contributes a sharp empirical demonstration of when the two spaces are *not* interchangeable: a weight-space modification projected through an activation-space basis loses approximately 97% of its energy.

3 Method

Notation. Let $W_{\text{base}}, W_{\text{fit}} \in \mathbb{R}^d$ denote the parameters of the base and fine-tuned models. Following Ilharco et al. [2], the *task vector* is the element-wise weight difference $\Delta W = W_{\text{fit}} - W_{\text{base}}$. We write

$W^{(l)}$ for the slice corresponding to layer $l \in \{1, \dots, L\}$. A Sparse Autoencoder at layer l provides an encoder–decoder pair (E_l, D_l) with D latent features; each column $d_{l,j}$ of D_l is interpreted as a feature direction. We use Gemma Scope 2 [6] with $D = 16,384$ features per layer in our primary experiments and $D = 262,144$ in our scale ablation.

Our method (Figure 1) consists of three steps: (i) extract a task vector via domain-specific LoRA fine-tuning; (ii) use SAE feature analysis to identify domain-specialized layers; and (iii) inject the raw, unfiltered task vector only into those layers.

Task vector extraction. We obtain ΔW via LoRA fine-tuning [1] on a domain-specific dataset. The selective injection pipeline is agnostic to the source of ΔW and would apply equally to task vectors from full fine-tuning.

SAE-guided layer selection. For each layer l and SAE feature j , we compare the feature’s mean activation on target-domain inputs to its mean activation on all other domains:

$$\text{spec}(l, j) = \frac{\bar{a}_{l,j}^{\text{target}}}{\bar{a}_{l,j}^{\text{other}} + \epsilon}, \quad (1)$$

with $\epsilon = 10^{-6}$. A feature is *domain-specific* if $\text{spec}(l, j) > \tau_f$ (we use $\tau_f = 1.0$). We aggregate feature-level specificity into a per-layer Specificity Score by taking the *maximum* rather than a count. Empirically the maximum is more discriminative than the count: it captures whether *any* highly-specialized feature exists in a layer, not merely how many low-specificity features happen to exceed a soft threshold. A layer with a single feature at $\text{spec}=10$ is more domain-relevant than a layer with twenty features at $\text{spec}=1.5$. The threshold $\tau_{\text{SP}} = 4.0$ was chosen on a held-out validation split and is ablated in Section 5.3.

$$\text{SP}(l) = \max_{j \in \{1, \dots, D\}} \text{spec}(l, j), \quad (2)$$

the maximum specificity over all SAE features in layer l . We select layers with $\text{SP}(l) \geq \tau_{\text{SP}}$, using $\tau_{\text{SP}} = 4.0$ in our main experiments, which yields 14 of 34 layers (Figure 2).

Selective raw task vector injection. Given selected layers $\mathcal{L}_{\text{selected}}$ and a global scaling parameter α :

$$W_{\text{new}}^{(l)} = \begin{cases} W_{\text{base}}^{(l)} + \alpha \cdot \Delta W^{(l)} & \text{if } l \in \mathcal{L}_{\text{selected}} \\ W_{\text{base}}^{(l)} & \text{otherwise.} \end{cases} \quad (3)$$

$\Delta W^{(l)}$ is the *unfiltered* per-layer task vector: no projection, no truncation, no SAE-based masking. Once applied, the edited model has identical architecture, parameter count, and inference cost to the base model. The optimal α is determined via grid search.

Why not project task vectors through SAE features? A natural alternative projects ΔW onto the subspace spanned by domain-specific SAE decoder vectors, $\Delta W_{\text{proj}}^{(l)} = \sum_{j \in \mathcal{F}_l} (d_{l,j}^\top \Delta W^{(l)} d_{l,j}) / (d_{l,j}^\top d_{l,j})$, where $\mathcal{F}_l = \{j : \text{spec}(l, j) > \tau_f\}$. Recall that task vectors ΔW modify the weights directly, while SAE decoder features $d_{l,j}$ describe directions in activation space, so any projection of ΔW through $d_{l,j}$ necessarily mixes two distinct spaces. In practice this retains only a few percent (roughly 2–3.5% across our SAE configurations) of the modification energy ($\|\Delta W_{\text{proj}}^{(l)}\|_F / \|\Delta W^{(l)}\|_F$) and systematically degrades performance (Section 5). The failure mode is geometric: SAE decoder vectors span the activation manifold at layer l , which is a different geometric object than the column space of $\Delta W^{(l)}$. Substituting one for the other introduces a representational mismatch [8]. We note that the near-total energy loss reported in Section 5 is the primary empirical evidence for this geometric mismatch; the mechanistic claim and the experimental observation are mutually consistent rather than independently derived.

4 Experimental Setup

Model and SAE. Gemma-3-4B-IT [7], a 4B-parameter instruction-tuned transformer with 34 layers. Gemma Scope 2 [6] provides pre-trained SAEs at every layer, with 16K features in main experiments and 262K in our scale ablation.

Per-Layer Number Theory Specificity (Gemma Scope 2, 16K features)

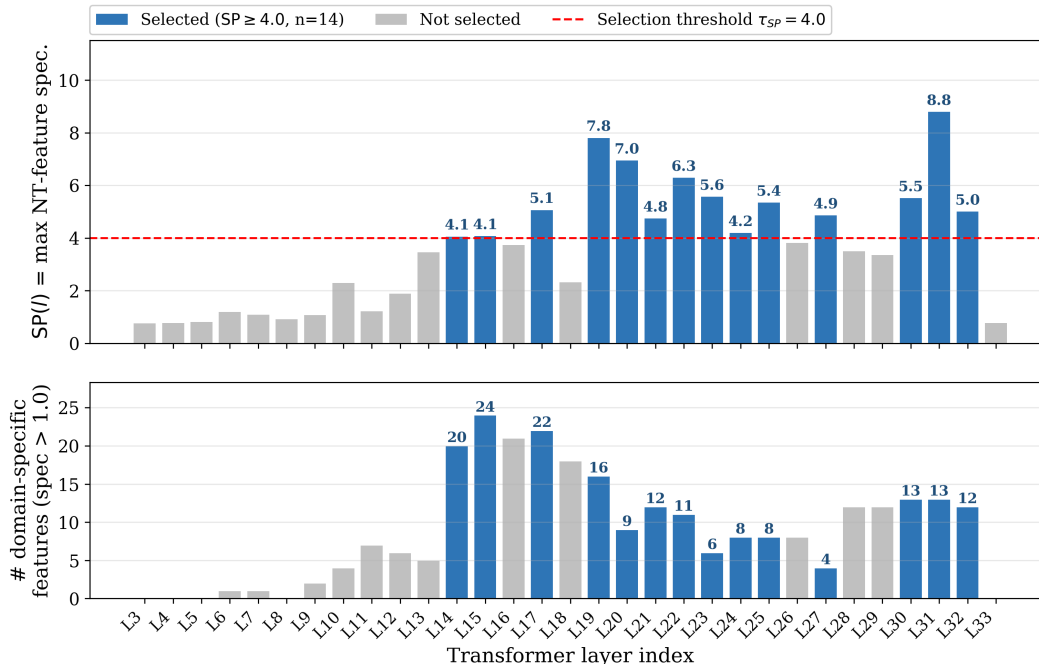


Figure 2: Per-layer Number Theory specificity (Gemma Scope 2, 16K features). *Top*: Specificity Score $SP(l) = \max_j \text{spec}(l, j)$ per layer; blue bars mark the 14 layers selected at $\tau_{SP} = 4.0$, the dashed red line indicates the threshold. *Bottom*: Number of domain-specific features ($\text{spec}(l, j) > 1.0$) per layer. The distribution is bimodal: a mid-network cluster (layers 14–17) and a late-network cluster (layers 30–32) carry the strongest domain specialization.

Task vector. Our primary task vector (v_2) is obtained by LoRA fine-tuning on 3,865 Number Theory problems from the MATH training set [12], with rank $r = 16$, learning rate 2×10^{-4} , and 5 epochs. Two alternatives (v_{25} : 6,155 samples; v_3 : 20,000 mixed-domain) test sensitivity to the source of ΔW (see appendix). For comparison against SAE projection in Section 5.4, we additionally define a smaller raw-injection control. The E3 baseline applies the raw task vector to a fixed seven-layer subset $\{19, 20, 22, 23, 25, 30, 31\}$ (configuration E3_7L in our codebase), chosen as the seven highest-SP layers among NT-analyzed layers in our initial sweep, rather than an SP threshold applied independently of rank. E3 isolates the contribution of layer *count* from the contribution of raw versus projected injection.

Evaluation. Minerva Math via lm-evaluation-harness [24]: 540 problems across 7 subjects (NT, CP, ALG, GEO, IA, PRE, PC). We use 4-shot prompting with greedy decoding and the `math_verify` metric.

Baselines. Three baselines share the same v_2 task vector: (i) **Base** (unmodified Gemma-3-4B-IT); (ii) **Full LoRA merge** (add ΔW to all 34 layers); (iii) **SAE Projection** (inject ΔW_{proj} into the same SP-selected layers). Each baseline’s α is independently grid-searched.

Statistical testing. Per subject we compute a two-sample proportion z -test: $z = (\hat{p}_{\text{edit}} - \hat{p}_{\text{base}}) / \sqrt{SE_{\text{edit}}^2 + SE_{\text{base}}^2}$, with two-sided p -values and significance at $|z| \geq 1.96$. Sample sizes are the full Minerva Math test sets: $n = 540$ (NT), 474 (CP), 1,187 (ALG), 479 (GEO), 903 (IA), 871 (PRE), 546 (PC). With these sample sizes the test is well-powered to detect effects of approximately 4 percentage points on every subject.

Determinism and hardware. All evaluations use greedy decoding with deterministic weight modifications; repeated runs of the same configuration produce identical accuracies at float64

Table 1: Performance on Minerva Math (7 subjects). Accuracy (%) and z -scores vs. base. **Bold**: statistically significant ($z \geq 1.96, p < 0.05$). †: best SAE-projected configuration (rank-3, $\alpha = 0.70$, 16K SAE). Ours: SP ≥ 4.0 layer selection (14/34 layers), $\alpha = 0.80$.

Method	NT	CP	ALG	GEO	IA	PRE	PC	#Sig
Base model	29.6	33.3	61.3	30.5	16.6	62.9	20.5	–
Full LoRA merge (34L)	30.0	33.8	58.1	29.2	16.3	61.4	19.8	0/7
SAE Projection†	33.9	34.6	62.1	31.0	16.8	63.5	20.3	0/7
Ours (SP4, $\alpha=0.80$)	39.4	41.4	67.0	37.2	19.6	69.6	20.5	5/7
z -score	+3.41	+2.56	+2.87	+2.19	+1.65	+2.94	+0.00	
p -value	0.0007	0.0105	0.0041	0.0286	0.0989	0.0032	1.0000	

precision (verified; Section 6). Experiments ran on $3 \times$ H100 80GB GPUs, totaling ~ 290 GPU-hours across reported configurations, plus an additional ~ 60 GPU-hours for the exploratory CMA-ES search reported in Appendix D (Figure 9).

5 Results

We organize results in four parts. Section 5.1 presents the main comparison against three baselines on Minerva Math (Table 1, Figure 3). Sections 5.2–5.4 isolate three design choices: the scaling parameter α , layer selection strategy, and—most critically—raw versus SAE-projected task vectors. Three findings stand out: (i) selective injection into 14 SAE-identified layers improves 5 of 7 math subjects with no degradation; (ii) performance is robust across a wide range of α but sensitive to layer selection above the threshold $\tau_{\text{SP}} = 4$; and (iii) projecting ΔW through SAE feature subspaces produces no statistically significant gains on any subject, despite retaining the same layer selection.

5.1 Main Results

Table 1 compares our method against three baselines sharing the same task vector source (v2). Our method achieves statistically significant improvements on 5 of 7 subjects, with the primary target (Number Theory) showing the strongest effect ($z = +3.41, p = 0.0007, +9.81$ pp absolute, $+33\%$ relative). Crucially, *no subject is degraded*: Intermediate Algebra is positive but does not reach significance ($p = 0.099$ two-sided); PreCalculus is unchanged. This demonstrates that selective injection avoids catastrophic forgetting without explicit regularization.

Two baselines fail to produce significant improvement on any subject. Full LoRA merge across all 34 layers actually *degrades* performance on Algebra (-3.2 pp), Geometry (-1.3 pp), and PreAlgebra (-1.5 pp), consistent with prior findings that uniform task-vector application introduces interference [13]. SAE Projection shows numerical improvements but none reach significance, despite using the *same layer-selection signal* as our method—confirming that the projection step itself, not layer selection, is the bottleneck (Figure 3).

5.2 Robustness to the Scaling Parameter

We searched $\alpha \in \{0.70, 0.75, \dots, 1.20\}$ for the SP4 14L configuration. The response surface is broad and flat: NT z -scores remain above $+2.84$ across the full range $\alpha \in [0.70, 1.10]$ (a 40% swing in scaling magnitude), with the peak at $\alpha = 0.80$ ($z = +3.41$) only marginally above the next-best values at $\alpha = 0.85$ ($z = +3.34$) and $\alpha = 0.70, 1.10$ ($z = +3.16$). Performance drops at $\alpha = 1.20$ ($z = +2.08$), marking the onset of over-modification. The empirical relationship $n_{\text{layers}} \times \alpha_{\text{opt}} \approx 11.2$ (14×0.80) for our configurations is consistent with a conserved “modification budget” across layer-selection strategies: Figure 6 shows the full SP4 14L response surface with the robust plateau annotated, and Figure 7 shows that SP4 noDeep (11 layers) reaches its peak at $\alpha^* = 1.00$, preserving the product $n_l \times \alpha^* \approx 11$. Full sweep and both figures in Appendix B.

5.3 Layer Selection Strategies

We compare six layer-selection strategies, each at its respective optimal α (Table 2). Three findings:

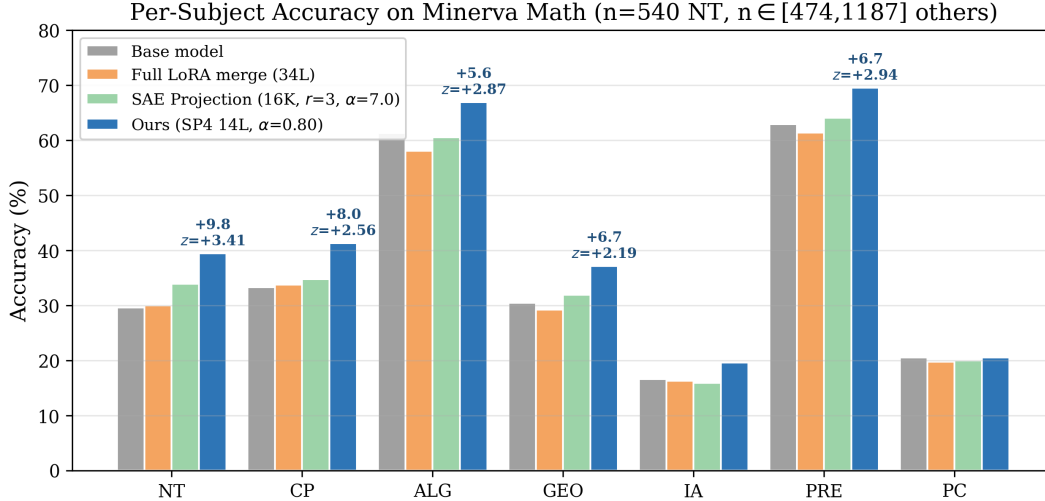


Figure 3: Per-subject accuracy across the seven Minerva Math subjects ($n = 540$ NT, $n \in [474, 1,187]$ others). Four conditions are shown left to right: Base model (leftmost/gray), Full LoRA merge 34L (middle left/orange), SAE Projection 16K (middle right/green), and Ours SP4 14L $\alpha=0.80$ (rightmost/blue). Our method achieves statistically significant gains on 5 of 7 subjects, with absolute improvements ranging from +5.6 pp on Algebra to +9.8 pp on Number Theory. Full LoRA merge degrades three subjects; SAE Projection (green bars) produces numerical shifts that do not reach significance on any subject, despite using the same layer-selection signal.

Table 2: Layer-selection strategy comparison. SP x denotes layers with Specificity Score $\geq x$. MID: layers 17–27. SP4_noDeep: SP4 with deep layers 30–32 removed. Each configuration uses its optimal α . Per-subject heatmap in Appendix C.

Configuration	#Layers	α^*	NT z	#Sig	Note
SP4 14L	14	0.80	+3.41	5/7	NT-best
SP4 noDeep	11	1.00	+3.22	6/7	Multi-subject best
SP3.5 17L	17	1.00	+2.33	6/7	Signal diluted
SP4 UNION	16	1.00	+2.33	6/7	Low-SP noise
MID 10L	11	0.90	+2.59	3/7	Missing deep layers
SP4.5 11L	11	1.00	+0.73	0/7	Excludes critical layers

The SP threshold matters more than layer count. Three configurations select roughly the same number of layers (11–14) but produce wildly different outcomes. SP4 14L ($z = +3.41$) and SP4 noDeep ($z = +3.22$) are both strong; SP4.5 11L collapses to $z = +0.73$ despite a similar layer count. Inspecting the SP4.5 selection reveals that raising the threshold from 4.0 to 4.5 excludes layers 14, 15, and 24, which carry essential domain computation. Lowering the threshold to $SP \geq 3.5$ (17 layers) dilutes the signal with weakly specialized layers ($z = +2.33$). The SP threshold acts as a categorical separator between domain-specialized and non-specialized layers, not a smooth knob.

Deep layers carry domain-specific but interference-prone modifications. Removing layers 30–32 trades NT performance ($z = +3.22$ vs. +3.41) for broader coverage (6/7 vs. 5/7 significant subjects), suggesting deep-layer task vectors encode NT-specific computations that mildly conflict with Intermediate Algebra.

Mid-layer heuristics are insufficient. The MID 10L configuration (a hand-chosen middle slab, layers 17–27) achieves only $z = +2.59$ on NT and 3/7 significant subjects. SAE-derived specificity identifies layers outside this range (notably 14, 15, and 30–32) that are critical to the effect. Per-subject z -scores across all six configurations are shown in Figure 8 (Appendix C).

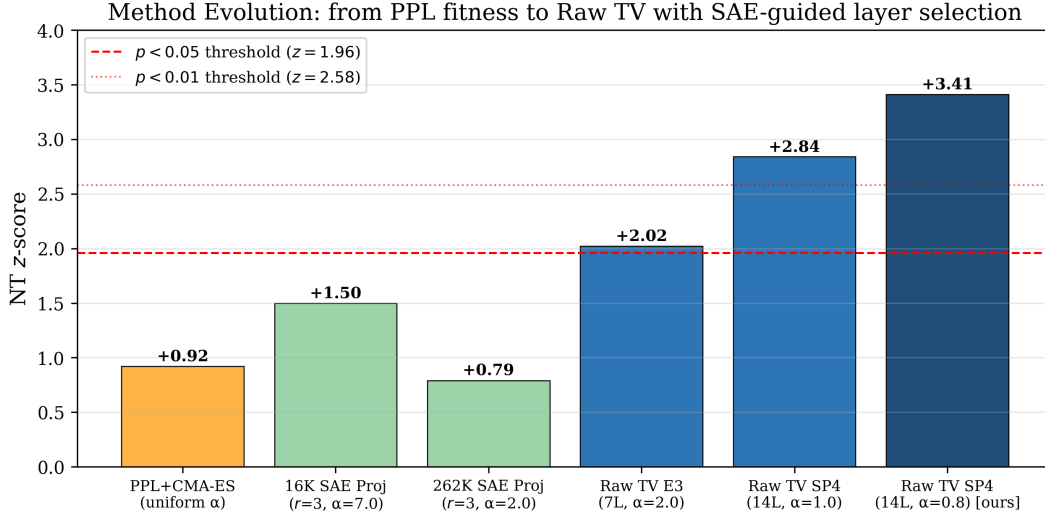


Figure 4: Method evolution: NT z -score across six approaches in order of development. PPL+CMA-ES with uniform α (orange) and both SAE Projection variants (green) remain below the $p < 0.05$ threshold ($z = 1.96$, red dashed line) and $p < 0.01$ threshold ($z = 2.58$, red dotted line). All three Raw Task Vector configurations (blue) cross into significance, with our final SP4 14L $\alpha=0.80$ reaching $z = +3.41$. The decisive transition is not feature width or layer count but whether the task vector is projected through SAE features before injection.

Table 3: Raw task vector vs. SAE-projected injection. “Energy retained” denotes $\|\Delta W_{\text{proj}}\|_F / \|\Delta W\|_F$. All configurations use the same v2 task vector. The $16\times$ increase in feature width does not close the gap. All p (NT) values are two-sided, using the same normal approximation as Table 1.

Method	Energy Retained	NT z	#Sig	p (NT)
SAE Proj (16K, rank-3)	$\sim 2.1\%$	+1.50	0/7	0.1336
SAE Proj (262K, rank-3)	$\sim 3.5\%$	+0.79	0/7	0.4296
Raw TV (E3, 7 layers)	100%	+2.02	1/7	0.0434
Raw TV (SP4, 14 layers)	100%	+3.41	5/7	0.0007

5.4 Raw Task Vectors versus SAE Projection

This section presents the central empirical claim of the paper: SAE projection systematically underperforms raw injection of the *same* task vector through the *same* layers (Table 3; cf. Figure 1 for the conceptual contrast), and across all 30+ configurations we tested no SAE-projected variant achieved a statistically significant gain on Number Theory.

Figure 4 traces the NT z -score across all six approaches in chronological order of development, from PPL+CMA-ES search through to our final Raw TV SP4 configuration; the transition into significance coincides exactly with the switch from SAE-projected to raw injection.

SAE projection at the standard 16K feature width retains only a few percent of the modification energy and produces no statistically significant improvement on any subject (NT $z = +1.50$, $p = 0.133$). Scaling to 262K features retains $\sim 3.5\%$ of the energy but NT performance *decreases* ($z = +0.79$, $p = 0.43$). The bottleneck is the projection step itself, not feature granularity. This is consistent with the geometric argument in Section 3: SAE decoder vectors span the activation manifold at layer l , a different geometric object than the column space of $\Delta W^{(l)}$.

The raw task vector injected into a smaller layer set (7 layers) achieves $z = +2.02$ ($p = 0.043$)—already outperforming both SAE-projection configurations despite using half as many layers. The decisive variable is therefore not how many layers receive the task vector, but whether the task vector is filtered through SAE features before injection. Figure 5 visualises this gap across all tested configurations: the $\sim 100\times$ difference in energy retention between SAE projection ($\leq 3.5\%$) and

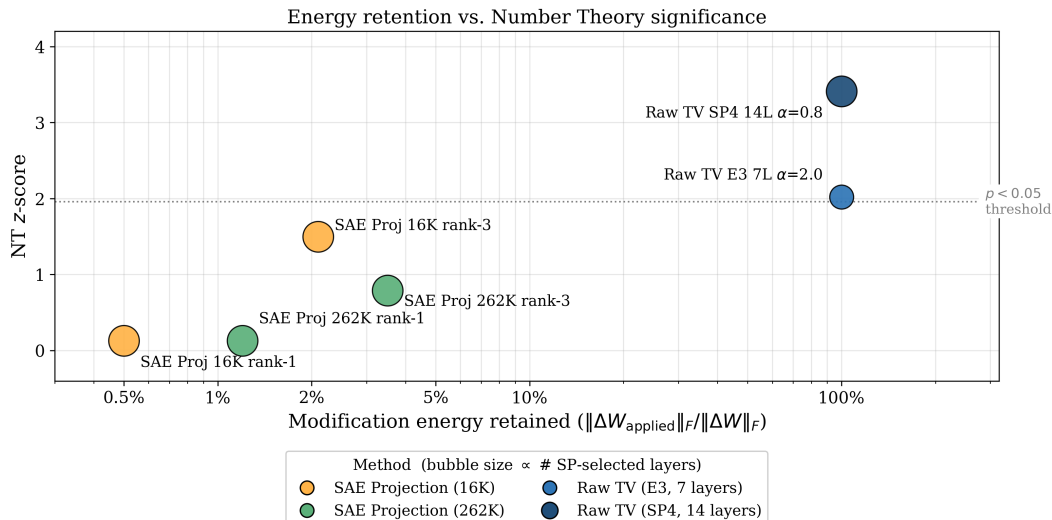


Figure 5: Energy retention vs. Number Theory significance (z -score) across all injection strategies (log-scale x -axis). Orange points: SAE Projection variants (16K and 262K features, rank-1 and rank-3); teal points: SAE Projection 262K variants; blue points: Raw Task Vector injection (E3 7-layer and SP4 14-layer). Bubble area is proportional to the number of SP-selected layers. Both raw-injection configurations exceed the $p < 0.05$ significance threshold (dotted horizontal line) while retaining 100% of $\|\Delta W\|_F$; no SAE-projected configuration does so at any feature width. The two-order-of-magnitude gap in energy retention ($\leq 3.5\%$ vs. 100%) is the proximate cause of the performance gap.

raw injection (100%) maps directly onto the difference between no significant result and $z = +3.41$. Across 30+ configurations, no SAE-projected variant we tested reached statistical significance on Number Theory; every raw-injection variant with ≥ 7 SP-selected layers did. This is strong evidence that SAEs should be used to identify *where* to edit, but not to filter *what* to inject.

6 Analysis and Discussion

6.1 SAEs as Diagnostic, Not Interventional, Tools

Recent work increasingly suggests that sparse autoencoders are more reliable as probes than as actuators, and our findings sharpen this pattern in the context of model editing. The central methodological claim of this work is that SAEs are useful for *identifying which layers to edit*, but not for *filtering what to inject into them*. Three lines of evidence support this: (i) replacing uniform task-vector application with SAE-derived layer selection moves NT z from $+0.13$ (Full LoRA merge) to $+3.41$, with 5/7 subjects significantly improved (Section 5.1); (ii) filtering ΔW through the SAE feature subspace, using the same layer selection, produces no statistically significant gain on any subject, even at $16\times$ feature width (Section 5.4); and (iii) SAE projection retains only a few percent of $\|\Delta W\|_F$ (up to $\sim 3.5\%$ even at $16\times$ feature width), and the bottleneck is geometric mismatch rather than feature granularity.

This pattern is consistent with a growing body of work on SAE limitations as intervention tools. Sharkey et al. [8] note that SAE reconstruction systematically loses information, and that SAEs decompose activations rather than the weights that compute them. Kantamneni et al. [9] show that SAE-based probes do not consistently outperform simple baselines. Heap et al. [10] find that SAEs trained on randomly initialized transformers produce features qualitatively similar to those from trained models. Fel et al. [21] argue that concepts in vision transformers may correspond to convex regions (the "Minkowski Representation Hypothesis") rather than linear directions; if this geometric structure is shared by language models (a hypothesis we cannot directly verify) then linear projection through SAE decoder vectors would be a lossy approximation. Our negative result is consistent with that prediction. Our finding fits this broader picture: SAEs encode genuine information about

layer-level specialization, but a linear projection onto SAE features is not a faithful representation of the weight-space modifications that drive fine-tuned behavior. The practical implication is a clean separation of roles—SAE for *where*, raw ΔW for *what*—which we expect to generalize beyond mathematical reasoning.

6.2 Deterministic Evaluation

We verified determinism by running the SP4 14L ($\alpha = 0.80$) configuration twice with identical specifications. All seven subject accuracies match at float64 precision (zero difference). Three properties guarantee this: (i) the task-vector application in Equation (3) involves only deterministic arithmetic; (ii) lm-evaluation-harness [24] uses greedy decoding with no sampling; and (iii) the `math_verify` metric is deterministic. The standard errors in our z -tests therefore arise entirely from finite-sample variation in the 540-problem benchmark, not from evaluation noise. The reported $p = 0.0007$ for Number Theory is a population-level statement, not a per-run estimate.

6.3 Additional Observations

Three further observations are documented in detail in the appendix: (i) during exploratory CMA-ES [25] optimization using perplexity (PPL) as a fitness signal, the lowest-PPL configuration was not the highest-accuracy one, motivating our switch to accuracy-based fitness for the rest of the search (Appendix D); (ii) combining NT and CP task vectors causes destructive interference even at modest scaling ($\alpha_{CP} = 1.0$: NT $z = -0.74$, ALG $z = -5.61$), suggesting partially overlapping weight subspaces (Appendix E); and (iii) task-vector quality depends on *domain focus* of the fine-tuning corpus, not size: a $5\times$ -larger mixed-domain corpus produced essentially no NT effect, while a focused 4,000-example corpus produced our best result (Appendix F). This mirrors prior editing and merging work that also uses task accuracy, rather than perplexity, as the primary fitness signal [2, 26].

7 Limitations

Single base model. All experiments use Gemma-3-4B-IT [7]. Our mechanistic argument should generalize across architectures, but we have not verified this empirically. Cross-model validation is feasible with currently available SAE suites: Llama Scope [20] provides full-layer SAE coverage for Llama-3.1-8B with 32K and 128K feature widths.

Single primary domain. The strongest claims concern Number Theory, with positive transfer to four other math subjects. Independent targeting of a more feature-dispersed domain (Counting & Probability, ~ 180 domain-specific features distributed across 18 layers) showed only marginal effects, suggesting the method’s effectiveness depends on whether the target domain has a sufficiently concentrated SAE-feature signature. Validation on non-mathematical domains (legal reasoning, code, multilingual translation) remains untested.

Absolute accuracy ceiling. Our edited model achieves 39.4% on Number Theory—a significant relative gain (+33%) but well below human expert performance. This reflects the capacity of the 4B base model rather than a limitation of the editing method.

Task vector prerequisite and SAE availability. The method requires one LoRA fine-tuning run (~ 4 GPU-hours, $\sim \$16$ at current cloud rates) and pre-trained SAEs at every layer. Comprehensive public SAE suites at this scale exist primarily for the Gemma family (Gemma Scope [5] and Gemma Scope 2 [6]) and the Llama family [20]. Training new SAEs is expensive (Gemma Scope used $\sim 15\%$ of Gemma 2 9B’s training budget [5]), but this cost is amortized: the same SAEs support unlimited downstream layer-selection queries. As with any capability-enhancing technique, our method could in principle be applied to harmful domains; we do not explore such applications and restrict ourselves to mathematical reasoning.

Statistical power. Subject-level z -tests are well-powered to detect ~ 4 pp effects on every subject given the full Minerva Math test set sizes ($n = 540$ NT; $n \in [474, 1,187]$ others). Intermediate Algebra ($z = +1.65$, $p = 0.099$, two-sided) does not reach significance and should be interpreted accordingly. PreCalculus ($z = 0.00$) shows no effect under this task vector.

8 Conclusion

We presented an interpretability-guided method for selective model editing that uses Sparse Autoencoder feature analysis to identify domain-specialized layers, then injects raw LoRA-derived task vectors into only those layers. On Gemma-3-4B-IT targeting Number Theory, the method achieves $z = +3.41$ ($p = 0.0007$), improving 5 of 7 math subjects with no degradation, and is fully deterministic at float64 precision.

The central scientific finding is methodological: **SAEs are useful as diagnostic tools for layer selection, not as intervention tools for filtering weight-space modifications.** Projecting task vectors through SAE feature subspaces—the intuitively obvious approach—retains only a few percent ($\leq 3.5\%$) of the modification energy and produces no statistically significant gain on any subject, even at $16\times$ feature width. The geometric reason is that SAE decoder vectors span the activation manifold while task vectors live in weight space; the two geometries are not interchangeable. The near-total energy loss is consistent with this structural incompatibility/geometric mismatch. Further, this finding is consistent with a growing body of work documenting SAE limitations as intervention tools [8–10] and contributes a sharp empirical demonstration of where the activation-space/weight-space distinction matters. Our results suggest that the efficacy of this diagnostic selection is contingent on the "sharpness" of the task vector itself: a $5\times$ larger mixed-domain corpus (v3) failed to produce a significant effect, reinforcing that surgical editing requires both precise layer selection and high-fidelity, domain-focused training data.

Future work includes cross-model validation using Llama Scope [20], extension to non-mathematical domains, integration with interference-mitigation strategies for multi-domain editing [13, 15], and a more principled characterization of when activation-space SAE analysis transfers cleanly to weight-space interventions versus when it fails. The broader implication is that interpretability tools and editing tools may serve complementary rather than substitutable roles—a separation we expect to generalize beyond the specific setting studied here.

References

- [1] Edward J Hu, Yelong Shen, Phillip Wallis, Zeyuan Allen-Zhu, Yuanzhi Li, Shengyu Wang, Lu Wang, and Weizhu Chen. LoRA: Low-rank adaptation of large language models. In *International Conference on Learning Representations (ICLR)*, 2022.
- [2] Gabriel Ilharco, Marco Tulio Ribeiro, Mitchell Wortsman, Suchin Gururangan, Ludwig Schmidt, Hannaneh Hajishirzi, and Ali Farhadi. Editing models with task arithmetic. In *International Conference on Learning Representations (ICLR)*, 2023.
- [3] Trenton Bricken, Adly Templeton, Joshua Batson, Brian Chen, Adam Jermyn, Tom Conerly, Nick Turner, Cem Anil, Carson Denison, Amanda Askell, et al. Towards monosemanticity: Decomposing language models with dictionary learning. *Transformer Circuits Thread*, 2023.
- [4] Hoagy Cunningham, Aidan Ewart, Logan Riggs, Robert Huben, and Lee Sharkey. Sparse autoencoders find highly interpretable directions in language models. *International Conference on Learning Representations (ICLR)*, 2024.
- [5] Tom Lieberum, Senthooan Rajamanoharan, Arthur Conmy, Lewis Smith, Nicolas Sonnerat, Vikrant Varma, János Kramár, Amos Drori, and Neel Nanda. Gemma scope: Open sparse autoencoders everywhere all at once on gemma 2. *arXiv preprint arXiv:2408.05147*, 2024.
- [6] Google DeepMind. Gemma scope 2: Sparse autoencoders and transcoders for gemma 3. *Technical report*, 2025. <https://deepmind.google/models/gemma/gemma-scope/>.
- [7] Gemma Team. Gemma 3 technical report. *arXiv preprint arXiv:2503.19786*, 2025.
- [8] Lee Sharkey, Bilal Chughtai, Dan Braun, Beren Millidge, et al. Open problems in mechanistic interpretability. *Transactions on Machine Learning Research*, 2025. arXiv:2501.16496.
- [9] Subhash Kantamneni, Joshua Engels, Senthooan Rajamanoharan, Max Tegmark, and Neel Nanda. Are sparse autoencoders useful? a case study in sparse probing. In *Proceedings of the 42nd International Conference on Machine Learning (ICML)*, volume 267, pages 29018–29049. PMLR, 2025.
- [10] Thomas Heap, Tim Lawson, Lucy Farnik, and Laurence Aitchison. Sparse autoencoders can interpret randomly initialized transformers. *arXiv preprint arXiv:2501.17727*, 2025.
- [11] Armaity Katki, Nathan Choi, Son Sophak Otra, George Flint, and Kevin Zhu. Where to edit? complementary protein property control from weight and activation spaces. In *NeurIPS 2025 Workshop on Biosecurity Safeguards for Generative AI (BioSafe GenAI)*, 2025. URL <https://openreview.net/forum?id=KiZxvtn3JE>.
- [12] Dan Hendrycks, Collin Burns, Saurav Kadavath, Akul Arora, Steven Basart, Eric Tang, Dawn Song, and Jacob Steinhardt. Measuring mathematical problem solving with the MATH dataset. *NeurIPS Datasets and Benchmarks*, 2021.
- [13] Prateek Yadav, Derek Tam, Leshem Choshen, Colin Raffel, and Mohit Bansal. TIES-merging: Resolving interference when merging models. In *Advances in Neural Information Processing Systems (NeurIPS)*, 2023.
- [14] Le Yu, Bowen Yu, Haiyang Yu, Fei Huang, and Yongbin Li. Language models are super mario: Absorbing abilities from homologous models as a free lunch. *arXiv preprint arXiv:2311.03099*, 2024.
- [15] Yifei He, Yuzheng Hu, Yong Lin, Tong Zhang, and Han Zhao. Localize-and-stitch: Efficient model merging via sparse task arithmetic. In *Transactions on Machine Learning Research (TMLR)*, 2025. arXiv:2408.13656.
- [16] Ronald Skorobogat, Karsten Roth, and Mariana-Iuliana Georgescu. Subspace-boosted model merging. *arXiv preprint arXiv:2506.16506*, 2025.
- [17] Kevin Meng, David Bau, Alex Andonian, and Yonatan Belinkov. Locating and editing factual associations in GPT. *Advances in Neural Information Processing Systems (NeurIPS)*, 2022.
- [18] Kevin Meng, Arnab Sen Sharma, Alex Andonian, Yonatan Belinkov, and David Bau. Mass-editing memory in a transformer. In *International Conference on Learning Representations (ICLR)*, 2023.
- [19] Guillermo Ortiz-Jiménez, Alessandro Favero, and Pascal Frossard. Task arithmetic in the tangent space: Improved editing of pre-trained models. In *Advances in Neural Information Processing Systems (NeurIPS)*, 2023.

- [20] Zhengfu He, Wentao Shu, Xuyang Ge, Lingjie Chen, Junxuan Wang, Yunhua Zhou, Frances Liu, Qipeng Guo, Xuanjing Huang, Zuxuan Wu, Yu-Gang Jiang, and Xipeng Qiu. Llama scope: Extracting millions of features from Llama-3.1-8B with sparse autoencoders. *arXiv preprint arXiv:2410.20526*, 2024.
- [21] Thomas Fel, Binxu Wang, et al. Into the rabbit hull: From task-relevant concepts in DINO to minkowski geometry. In *International Conference on Learning Representations (ICLR)*, 2026. arXiv:2510.08638.
- [22] Ekdeep Singh Lubana et al. Priors in time: Missing inductive biases for language model interpretability. *arXiv preprint arXiv:2511.01836*, 2025. ICLR 2026 poster.
- [23] Wen Lai, Alexander Fraser, and Ivan Titov. Joint localization and activation editing for low-resource fine-tuning. In *Proceedings of the 42nd International Conference on Machine Learning (ICML)*, volume 267, pages 32206–32227. PMLR, 2025.
- [24] Leo Gao, Jonathan Tow, Baber Abbasi, Stella Biderman, Sid Black, Anthony DiPofi, Charles Foster, Laurence Golding, Jeffrey Hsu, Alain Le Noac’h, et al. A framework for few-shot language model evaluation. *Zenodo*, 2024.
- [25] Nikolaus Hansen. The CMA evolution strategy: A comparing review. *Towards a New Evolutionary Computation*, pages 75–102, 2006.
- [26] Takuya Akiba, Makoto Shing, Yujin Tang, Qi Sun, and David Ha. Evolutionary optimization of model merging recipes. *arXiv preprint arXiv:2403.13187*, 2024.

A Reproduction Commands

```
# Step 1: LoRA fine-tuning (produces task vector v2)
python experiments/nt_train_lora_v2.py \
    --gpu 0 --name lora_v2 --epochs 5 --lora_r 16

# Step 2: Compute task vector and apply to SP>=4.0 layers
python experiments/raw_tv_sweep_v2.py \
    --config SP4_14L --alpha 0.80 --tv v2

# Step 3: Evaluate with lm-eval
lm_eval --model hf \
    --model_args pretrained=results/raw_tv_v2/models/SP4_14L_a0.8 \
    --tasks minerva_math_* --num_fewshot 4 --batch_size 4
```

The commands above document the script-level invocation pattern used in our experiments. Implementation code is proprietary and is not released with this submission. The methodology is fully specified by Section 4 (training hyperparameters), Section 3 (algorithm), and Appendix H (per-layer specificity scores), enabling independent re-implementation against publicly available assets.

B Alpha Response Curve: Full Sweep

Table 4 reports the full alpha sweep for the SP4 14L configuration referenced in Section 5.2. Figures 6 and 7 visualize the response surface for SP4 14L alone and in comparison with SP4 noDeep (11 layers).

Table 4: Alpha response curve for the SP4 14L configuration. NT accuracy and z -scores as a function of α . The response surface is robust over a wide range ($z \geq 2.84$ for $\alpha \in [0.70, 1.10]$); only $\alpha = 1.20$ shows substantial degradation.

α	NT Acc	NT z	CP z	ALG z	GEO z	#Sig
0.70	38.7%	+3.16	+2.5	+3.0	+2.5	4/7
0.75	38.3%	+3.03	+2.5	+2.8	+2.0	5/7
0.80	39.4%	+3.41	+2.6	+2.9	+2.2	5/7
0.85	39.3%	+3.34	+2.7	+2.9	+2.6	5/7
0.90	37.8%	+2.84	+2.8	+3.2	+2.7	5/7
1.10	38.7%	+3.16	+2.7	+2.8	+1.8	4/7
1.20	35.6%	+2.08	+2.6	+2.4	+2.3	5/7

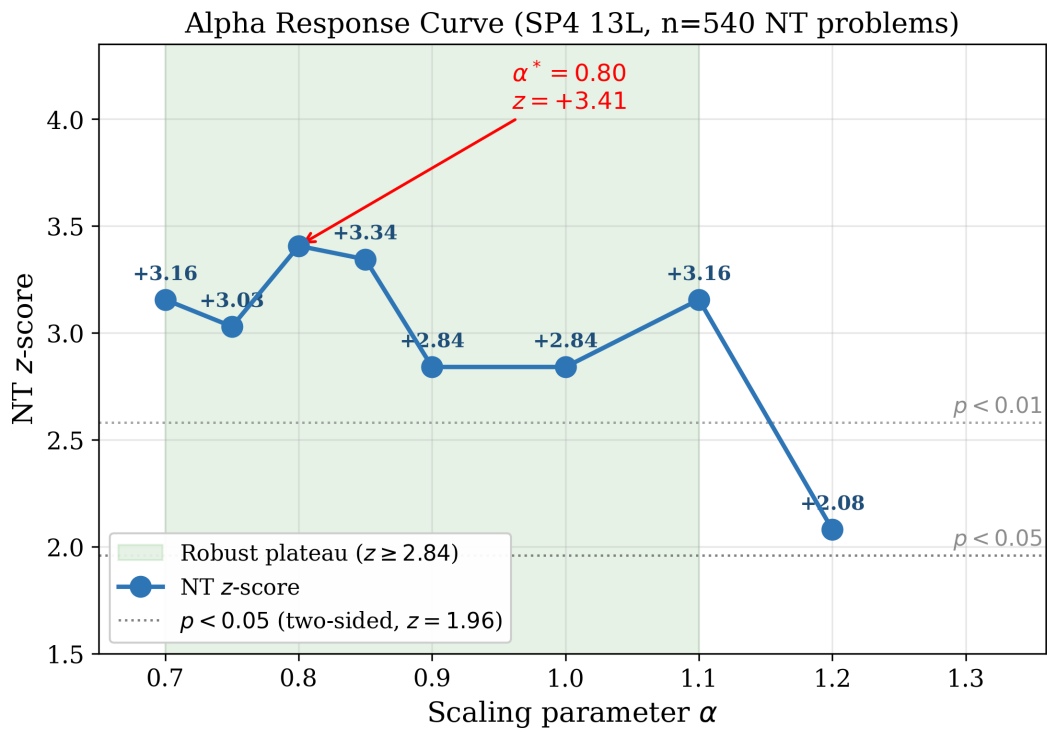


Figure 6: Number Theory z -score as a function of α for the SP4 14L configuration ($n = 540$ NT problems). The green shaded region marks the robust plateau ($z \geq 2.84$, $\alpha \in [0.70, 1.10]$). The optimal $\alpha^* = 0.80$ ($z = +3.41$) is annotated in red. Two dotted reference lines indicate the $p < 0.05$ ($z = 1.96$) and $p < 0.005$ ($z = 2.58$) thresholds. Performance drops sharply only at $\alpha = 1.20$, marking the onset of over-modification.

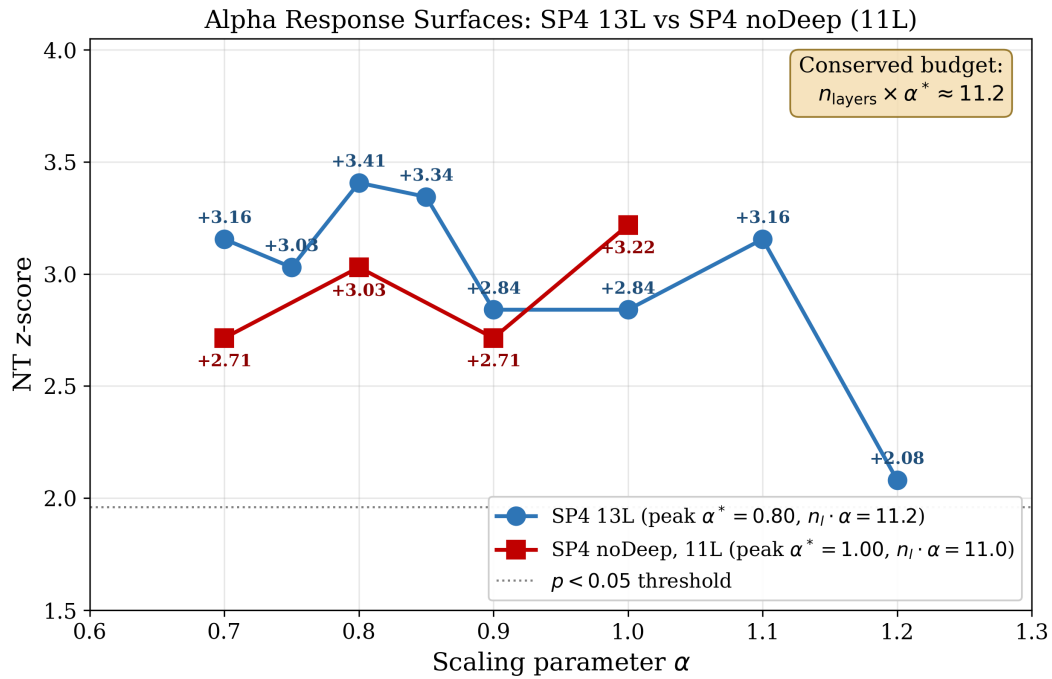


Figure 7: Alpha response surfaces for SP4 14L (blue circles, 14 layers) and SP4 noDeep (red squares, 11 layers). Both configurations peak within the same z-score range despite different layer counts: SP4 14L at $\alpha^* = 0.80$ ($n_l \times \alpha^* = 11.2$) and SP4 noDeep at $\alpha^* = 1.00$ ($n_l \times \alpha^* = 11.0$). The near identical products ($n_{\text{layers}} \times \alpha^* \approx 11.2$) are consistent with the interpretation that α compensates for reduced layer coverage rather than independently controlling edit strength.

C Layer Selection: Per-Subject Heatmap

Figure 8 shows per-subject z -scores for the six representative layer-selection configurations referenced in Section 5.3.



Figure 8: Per-subject z -scores across six layer-selection configurations. SP4 14L and SP4 noDeep dominate across most subjects; SP4.5 11L collapses to non-significance despite a similar layer count, showing that the SP threshold acts as a categorical separator rather than a smooth knob.

D Perplexity as a Fitness Metric

During an exploratory CMA-ES [25] optimization of per-layer α values (~ 60 GPU-hours), we used held-out perplexity (PPL) as a proxy fitness signal and subsequently evaluated the top configurations on accuracy. The top three configurations spanned only ~ 0.4 PPL points but differed by ~ 1.3 percentage points in NT accuracy, and the lowest-PPL configuration was not the highest-accuracy one. With $n = 3$ configurations in this range, the within-search correlation is too weak to support a generalizable claim, but the observation was sufficient to motivate switching to accuracy-based fitness. Figure 9 shows the PPL–accuracy relationship for both the CP and NT CMA-ES searches: Pearson $r = -0.06$ for CP and $r = +0.14$ for NT, both consistent with no reliable correlation.

The structural reason PPL and accuracy can diverge is that PPL is a token-level average over a corpus distribution, whereas mathematical accuracy is a sequence-level boolean over chain-of-thought completions. A model can produce fluent but incorrect reasoning chains and achieve low PPL; conversely, a model that solves problems correctly may produce slightly more “surprising” tokens than the base distribution. Our practical conclusion, which is to use accuracy directly as the fitness metric, is consistent with prior practice in evolutionary merging [26] and task arithmetic [2]. Whether PPL is a reliable fitness signal for non-mathematical model editing remains an open question.

E Cross-Domain Interference in Multi-Task Injection

We tested whether two domain-specific task vectors could be combined additively. Combining the NT task vector with a Counting & Probability (CP) task vector at modest scaling ($\alpha_{CP} = 0.5$) reduced NT performance from $z = +3.41$ to $z = +2.65$ (3/7 significant), while increasing CP scaling to $\alpha_{CP} = 1.0$ caused catastrophic collapse: NT $z = -0.74$ (accuracy roughly unchanged). Under DUAL (SP4 NT + CP task vectors, both at $\alpha=1.0$), Algebra (`math_verify`) falls from **61.3%** to $\sim 50.0\%$ (base model vs. edited model on the same 1,187-problem ALG split), with $z_{ALG} = -5.61$.

PPL fitness is not predictive of accuracy in CMA-ES top-3 (CP $r = -0.06$, NT $r = +0.14$; $n=3$ each, no linear fit shown)

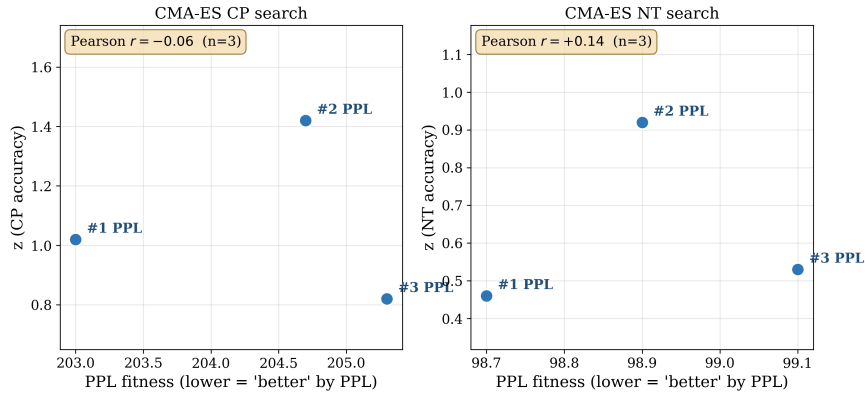


Figure 9: PPL fitness vs. accuracy z -score for the top-3 CMA-ES configurations in the CP search (left) and NT search (right). Each point is one configuration ranked by PPL fitness (lower PPL = “better” by the fitness signal). Red dashed lines show the Pearson regression fit. CP: $r = -0.06$ (essentially uncorrelated); NT: $r = +0.14$ (slightly positive, opposite to the anti-correlation the fitness signal assumes). In both searches the lowest-PPL configuration (#1 PPL) is *not* the highest-accuracy one, motivating our switch to accuracy-based fitness for the remainder of the search.

This indicates that NT and CP task vectors occupy partially overlapping weight subspaces and cannot be simply summed without destructive interference.

This is consistent with prior findings on task-vector interference [13, 15] and motivates integration with existing interference-mitigation strategies. The SP-based layer selection identifies ≥ 14 layers per domain, and these sets overlap substantially across NT and CP. Future work could combine SAE-guided layer selection with TIES-style sign-conflict resolution [13] or DARE-style random dropping [14].

F Task Vector Source: Data Quality Over Quantity

We compared task vectors trained on three datasets:

- **v2**: 3,865 NT-focused samples \rightarrow NT $z = +3.41$ (5/7 significant).
- **v25**: 6,155 samples (NT-focused, broader) \rightarrow NT $z = +2.84$, ALG $z = +4.07$.
- **v3**: 20,000 mixed-domain samples \rightarrow NT $z = +0.46$ (0/7 significant).

More data does not produce better task vectors for the target subject. The $5\times$ -larger mixed-domain corpus (v3) yields a task vector essentially indistinguishable from no edit on Number Theory. The intermediate v25 corpus ($1.6\times$ the v2 size, broader content) trades NT performance for stronger transfer to Algebra. This indicates that the domain focus of the fine-tuning corpus, not its size, determines the target-domain content of the resulting task vector.

G Configuration Rankings

Table 5 reports the top 10 configurations across all 30+ ablations evaluated with full lm-eval (540 problems, math_verify metric). All configurations use the v2 task vector unless noted.

H Per-Layer Specificity Scores

Table 6 lists the number of domain-specific features (specificity > 1.0) per layer for Number Theory, as identified by Gemma Scope 2 [6] with 16K features per layer. Layers with SP ≥ 4.0 (selected for injection) are marked.

Table 5: Top-10 configurations by NT z -score. “DUAL” denotes combined NT and CP task vectors. “v25” denotes the 6155-sample task vector variant.

Rank	Configuration	α	NT z	#Sig	Note
1	SP4 14L	0.80	+3.41	5/7	Global optimum
2	SP4 noDeep	1.00	+3.22	6/7	Multi-subject best
3	SP4 14L	0.70	+3.16	4/7	
3	SP4 14L	1.10	+3.16	4/7	
5	DUAL MID+CP0.5	1.00	+3.09	4/7	DUAL config
6	SP4 14L	0.90	+2.84	5/7	
6	SP4 14L	1.00	+2.84	5/7	
6	v25 SP4 14L	1.00	+2.84	5/7	6155-sample TV
9	MID 10L	0.90	+2.59	3/7	
9	MID 10L	1.00	+2.59	2/7	

Table 6: Per-layer Number Theory specificity score $SP(l) = \max_j \text{spec}(l, j)$ computed using Gemma Scope 2 SAEs with 16K features per layer. Layers with $SP(l) \geq 4.0$ (selected for raw task vector injection) are marked with \bullet . The companion column “#feat” shows the number of features with $\text{spec}(l, j) > 1.0$ in each layer (used in Figure 2 bottom panel).

Layer	SP	#feat	Sel.	Layer	SP	#feat	Sel.
L6	1.21	1		L20	7.00	9	\bullet
L7	1.10	1		L21	4.75	12	\bullet
L9	1.08	2		L22	6.30	11	\bullet
L10	2.30	4		L23	5.58	6	\bullet
L11	1.23	7		L24	4.21	8	\bullet
L12	1.90	6		L25	5.35	8	\bullet
L13	3.47	5		L26	3.83	8	
L14	4.07	20	\bullet	L27	4.88	4	\bullet
L15	4.09	24	\bullet	L28	3.52	12	
L16	3.74	21		L29	3.37	12	
L17	5.08	22	\bullet	L30	5.54	13	\bullet
L18	2.33	18		L31	8.80	13	\bullet
L19	7.82	16	\bullet	L32	5.02	12	\bullet

I Broader Impacts

This work develops methods for surgical model editing of existing language models. We see two principal positive implications: (i) the method enables targeted capability enhancement at substantially lower compute cost than full fine-tuning, reducing the carbon footprint of model specialization; (ii) the negative result on SAE projection clarifies what interpretability tools can and cannot reliably do for editing applications, supporting more rigorous use of mechanistic-interpretability tooling in practice.

We see one principal risk worth flagging: targeted model editing techniques can in principle be applied to enhance capabilities for harmful purposes, in the same way that any fine-tuning method can. Our method is no more dual-use than LoRA fine-tuning itself, which is widely available. We do not release new model weights, datasets, or capabilities beyond what is already publicly accessible.

J Licenses for Used Assets

This work uses the following publicly available assets:

- Gemma-3-4B-IT model [7]: Gemma Terms of Use (<https://ai.google.dev/gemma/terms>).
- Gemma Scope 2 SAEs [6]: CC-BY-4.0 (per the Hugging Face release).
- MATH dataset [12]: MIT License.
- lm-evaluation-harness [24]: MIT License.

We use each asset within the scope permitted by its respective license.